Annals of Biomedical Engineering, Vol. 29, pp. 284–297, 2001
Printed in the USA.

0090-6964/2001/29(4)/284/14/$15.00

Numerical Simulation of Enhanced External Counterpulsation

EDWIN T. OZAWA, KAREN E. BOTTOM, XINSHU XIAO, and ROGER D. KAMM

Department of Mechanical Engineering, Fluid Mechanics Laboratory, Massachusetts Institute of Technology, Cambridge, MA

(Received 7 April 2000; accepted 24 January 2001)

Abstract—Enhanced external counterpulsation (EECP) is a noninvasive, counterpulsative method to provide temporary aid to the failing heart by sequentially inflating cuffs on the lower extremity out-of-phase with the left ventricle. Optimization of the method necessitates consideration of the hemodynamics created by EECP and the mode of action providing patient benefit. A computational model based on the governing one-dimensional equations is developed that simulates cardiovascular hemodynamics during EECP. The model includes a 30-element arterial system including the left ventricle, bifurcations, and peripheral arterial vessels. Effects of vessel collapse as external pressure is applied, arterial refilling on pressure release, changes in aortic pressure, and shear stress generated in the arteries are each investigated. Device parameters are systematically varied to determine their effect on system performance. Results show the potential for significant collapse and shear augmentation throughout the arteries of the lower extremity. Performance is strongly influenced by the mean level of external pressurization and the timing of cuff inflation, but less so by the relative timing and pressure differences between cuff segments. © *2001 Biomedical Engineering Society.* [DOI: 10.1114/1.1359448]

Keywords—Cardiac assist, Computational model, Revascularization, Cardiovascular system.

INTRODUCTION

Enhanced external counterpulsation (EECP) is a noninvasive, counterpulsative procedure providing temporary support for the failing heart. EECP involves surrounding the lower half of a patient's body (lower abdomen, thighs, and calves) with inflatable cuffs that are pressurized and depressurized approximately out-of-phase with the left ventricle. While the aortic valve is closed (ventricular diastole), pressurization of the cuffs collapses the arteries causing the blood stored in the lower extremities to be directed retrograde toward the heart. The resultant increase in aortic diastolic pressure has the potential to increase blood flow to vital organs, especially the heart, which receives much of its perfusion during diastole. Just prior to ventricular ejection (systole), the cuffs are depressurized to atmospheric pressure and the collapsed arteries begin to refill. This causes a rarefaction wave to propagate retrograde reaching the heart during cardiac systole, thereby decreasing cardiac afterload.

EECP has been tested as a means of cardiac assist in patients suffering from cardiogenic shock[22] and acute myocardial infarction,[19] and as treatment for cardiac ischemia and angina.[15,16,31] Despite some success in these trials EECP is not currently used as a means of cardiac assist. It is, however, gaining acceptance as a treatment for patients suffering from cardiac ischemia and severe angina secondary to coronary disease[1,16,30] based on strongly favorable results from a recent multicenter study.[4]

Despite this success, the mechanisms by which EECP reduces angina and improves cardiac function remain unclear. It has been proposed that factors other than the purely mechanical ones may be responsible, and that EECP may enhance the development of collateral vessels in the coronary circulation. For example, Soran *et al.* recently argued that the beneficial effects of EECP might be a consequence of angiogenic factors released as a result of increased shear stress.[21]

Here we extend that thesis, and propose that the vascular (endothelial and/or smooth muscle) cells of the lower extremity may be a source of these factors since the enhancement in shear stress is far more dramatic there than elsewhere in the circulation, and the endothelial surface area quite large. We therefore consider not only the changes in aortic root pressure as it relates to direct, mechanical cardiac effects and coronary blood flow, but also arterial collapse and the augmentation of hemodynamic shear stress that accompany lower extremity compression. A new cardiovascular fluid mechanics model is presented that allows us to simulate the hemodynamics associated with EECP to determine how the operating parameters of the device influence its performance.

METHODS

Governing Equations. Following Stettler *et al.*,[23] we consider the one-dimensional form of the equations of mo-

Address correspondence to Roger D. Kamm, M.I.T., Room 3-260, 77 Massachusetts Ave., Cambridge, MA 02139. Electronic mail: rdkamm@mit.edu

tion since we are interested in the mean values of pressure and flow at specific locations in the arteries. Furthermore, higher dimensional flow problems are at present too computationally expensive to be of practical use. One-dimensional flow in an elastic artery can be described using the basic equations for momentum and continuity:

$$\frac{\partial}{\partial t}[\mathbf{A}]+\frac{\partial}{\partial x}[\mathbf{B}]+[\mathbf{C}]=0, \tag{1}$$

where

$$[\mathbf{A}]=\begin{bmatrix} u \\ A \end{bmatrix}, \tag{2}$$

$$[\mathbf{B}]=\begin{bmatrix} u^2/2+P/\rho \\ uA \end{bmatrix}, \tag{3}$$

and

$$[\mathbf{C}]=\begin{bmatrix} F \\ \Psi \end{bmatrix}, \tag{4}$$

where u and P are the local cross-sectional average velocity and pressure, A is the cross-sectional area, and F is the frictional loss, to be described later in further detail. The term Ψ representing minor branch flow in the continuity expression represents the distributed outflow per unit length and is approximated as a linearly resistive element, described by the equation

$$\Psi(P,x)=\Phi(x)(P-P_v). \tag{5}$$

Here the driving force for flow is the pressure drop between the local arterial pressure and the uniform venous pressure P_v. The constant $\Phi(x)$ describes the spatial distribution of flow into smaller branches.

A pressure–area relation or "tube law" may be formulated to provide a third independent equation. This relationship will be described below. The set of hyperbolic, partial differential equations in Eq. (1) for the arterial elements are solved using an adaptation of the MacCormack two-step predictor–corrector method.[2]

The expression for the frictional loss F in Eq. (4) may be derived as follows. The general form of the frictional or viscous loss term is given by the expression

$$F=-\frac{2\tau_0}{\rho R}, \tag{6}$$

where R is the arterial radius. From Young and Tsai[29] the shear stress term may be represented as

$$\tau_0=\frac{4C_v\mu}{R}\cdot u(t)+\frac{\rho}{2\pi R}\cdot(C_u-1)\cdot\frac{\partial Q}{\partial t}, \tag{7}$$

where C_u and C_v are functions of the local frequency parameter α:

$$\alpha=R_0\cdot\sqrt{\frac{\omega}{v}}. \tag{8}$$

Here R_0 is the arterial radius, ω is the angular frequency of oscillation, and v is the kinematic viscosity of the fluid. Young and Tsai[29] give plots of C_u and C_v versus α, from which algebraic approximations were generated for use in the model.

A hybrid tube law was used to describe the relationship between arterial cross-sectional area and transmural pressure. During arterial collapse, the steady state shear term in Eq. (7) is increased by a factor of 3 to reflect the change in cross-sectional shape.[14] We also modify the tube law used by Stettler *et al.*[23] to avoid a singularity that arises at negative transmural pressures. The modified forms are used when $A/A_0<0.36$, where A_0 is the area at a reference pressure $P_0=100\,\text{mm Hg}$ (13.3 kPa) and has the form

$$P_{\text{tm}}=P_{\text{tm}}(A)+\eta\frac{\partial A}{\partial t}. \tag{9}$$

Here the transmural pressure P_{tm} is the difference between the internal and external pressures across the artery wall and is related to the cross-sectional area through the expressions given in Table 1. The term $P_{\text{tm}}(A)$ in Eq. (9) represents the elastic response associated with a static transmural pressure, and η is a damping coefficient. A value of $2.0\times10^5\,\text{N s m}^{-4}$ was used for η in the model, selected based on comparisons to a previous, somewhat more rigorous model for viscoelasticity[11] as described in Bottom.[10] The actual form of the tube law expressing area as a function of pressure is solved using a binomial expansion approximation applied to Eq. (9). The equations required for calculation of the hybrid tube law are summarized in Table 1 for both the collapsed and uncollapsed regimes.

Bifurcations. The individual arterial segments are coupled through appropriate boundary conditions. At bifurcations where a single tube branches into separate daughter tubes we write the equation of energy conser-

TABLE 1. Forms used to describe the elastic response of the artery in the numerical solution. Different forms were required to capture the behavior of the distended ($A \geq A_T$) and collapsed ($A < A_T$) vessels.[a–e]

Inverse tube law	$A \geq A_T$	$P_{tm} = \left[\dfrac{P_0 + \rho c_0 g(z) \chi_0 \ln\left(\dfrac{A}{A_0}\right)}{1 - \rho c_0 B g(z) \ln\left(\dfrac{A}{A_0}\right)} \right] + \eta \dfrac{\partial A}{\partial t}$
	$A < A_T$	$P_{tm} = P_0 + \rho c_0 g(z)(\chi_0 + B P_T) \ln\left(\dfrac{A}{A_0}\right) + \eta \dfrac{\partial A}{\partial t}$
Elastic response	$A \geq A_T$	$A^s = A_0 \exp\left[\dfrac{P_{tm} - P_0}{\rho c_0 c(P,z)}\right]$
	$A < A_T$	$A^s = A_0 \exp\left[\dfrac{P_{tm} - P_0}{\rho c_0 g(z)(\chi_0 + B P_T)}\right]$
Wave speed	$A \geq A_T$	$c(P,z) = g(z)(\chi_0 + B P_{tm})$
	$A < A_T$	$c(P,z) = \sqrt{g(z) c_0 (\chi_0 + B P_T)}$

[a]Condition for collapse is $A < A_T$, where A is the cross-sectional area, and A_T is the transitional area, $A_T = 0.36 A_0$.
[b]P_{tm} is the transmural pressure.
[c]P_0 is the reference pressure, equal to 100 mm Hg (13.3 kPa).
[d]A_0 is the elastic response at the reference pressure P_0.
[e]The constants B, χ_0, and the function $g(z)$ are obtained from experimental measurements as described in Stettler *et al.* (Ref. 23).

vation for a control volume corresponding to a stream tube that includes all of the flow entering the nth daughter branch[28]

$$\rho \frac{\partial u_1}{\partial t} x_1 + \rho \frac{\partial u_n}{\partial t} x_n + P_n + \frac{1}{2} \rho (u_n^2 f_n + u_n |u_n| k_n) - P_1 - \frac{1}{2} \rho u_1^2 + \frac{1}{2} \rho u_n |u_1 u_n|^{1/2} \lambda_n = 0, \tag{10}$$

where the subscript "1" denotes the parent branch and the subscript "n", one of the daughter branches. The absolute values of velocity are incorporated to preserve the directionality of the losses as the flow changes direction. The unsteady continuity equation for the control volume encompassing the entire bifurcation including all daughter vessels is written as

$$\frac{\partial A_1}{\partial t} x_1 + \frac{\partial A_2}{\partial t} x_2 + \ldots + \frac{\partial A_N}{\partial t} x_N - u_1 A_1 + u_2 A_2 + \ldots + u_N A_N = 0, \tag{11}$$

where N is the total number of elements connected at a bifurcation, including the parent branch. The equations of motion coupled with momentum, continuity, and the hybrid tube law are applied at the interface between an element and the bifurcation control volume.

The term f_n in Eq. (10) representing the ratio of actual kinetic energy flux at n to that corresponding to a flat velocity profile is assumed to approach unity in the parent branch. The coefficients λ_n and k_n are dimensionless head loss coefficients due to "entrance type" and "turbulent type" losses, respectively. Following Pedley *et al.*,[20] λ_n is given by

$$\lambda_n = \frac{16C}{\sqrt{2}} \left[\frac{1}{\mathrm{Re}_1} \frac{D_1}{D_n} \frac{L_n}{D_n} \right]^{1/2}, \tag{12}$$

where Re_1 is the Reynolds number of the parent branch, C is a constant, D_1 and D_n are the diameters for the parent branch and nth daughter branch, respectively, and L_n is the entrance length for the nth daughter branch.

Values of the kinetic energy and dissipation factors are dependent on the nature of flow at the bifurcation. These loss coefficients are approximated by Wolf as[28]

$$k_n = \left(1 - \frac{1}{K_{c,n}}\right)^2 \tag{13}$$

and

$$f_n = \left(\frac{1}{K_{c,n}}\right)^2. \tag{14}$$

The contraction coefficient $K_{c,n}$ represents the ratio between the minimum normal cross-sectional area of the streamtube within the separated region of the nth daughter branch, and the area of the branch itself. Hence, for smaller angles between adjacent daughter branches, separation does not occur and $K_{c,n}$ should approach unity. Using literature values for the anatomical branching angles of the arterial system, a linear relationship between angle and $K_{c,n}$ is assumed and values assigned for each branch. The method is imprecise, however a sensitivity analysis of the contraction coefficients demonstrates that exact values are not required due to their small effect on the system as a whole. The energy conservation equation [Eq. (10)], and the unsteady form of continuity [Eq. (11)] are solved by the MacCormack predictor–corrector computational scheme,[1] coupling the state variables of the bifurcation end nodes with the internal points of the involved arterial elements.

Ventricle. A model of the left ventricle acts as an upstream boundary for the arterial tree. The ventricle may be approximated as a chamber whose compliance (or the inverse of elastance) changes with time, thus driving flow through a unidirectional exit valve into the aorta. Following the work of Suga and Sagawa,[24] the specified elastance curve $E(t)$ is used to characterize ventricular ejection and filling. Extensive studies of the pressure–volume relationship in canine ventricles[24] have shown that the basic shape of the systolic portion of the pressure–volume curve remains unchanged, regardless of loading or wall compliance changes. Thus, the systolic wall elastance may be characterized by only two parameters; the peak wall elastance $E_{\max}$ and time to this peak elastance during one cycle $T_{\max}$. The duration of the cycle is extrapolated from Suga and Sagawa's data suggesting that $T_{\max}$ spans approximately 30%–50% of the total cycle.

In a later extension of this model by Suga and Sagawa,[25] the effects of myocardial viscoelasticity were taken into account by the addition of one term to the ventricular pressure–volume relation. We found this approach to better fit data for humans[18] and have consequently used the following form in the present simulations:

$$P_{\text{vent}} = E^*(t)\cdot(V_{\text{vent}} - V_{\text{vent},0})\cdot\left[1+\sigma\left(\frac{dV_{\text{vent}}}{dt}\right)\right] + P_{\text{tp}}. \tag{15}$$

The coefficient σ is a scaling factor for the time-dependent viscoelastic effects, P_{vent} is the ventricular volume, V_{vent} is ventricular volume, $V_{\text{vent},0}$ is the zero-pressure filling volume, and P_{tp} is the transpulmonary pressure in the chest cavity which is expected to alter the left ventricular transmural pressure. We define the isovolumetric contraction curve $E^*(t)$ and assume it to be a half sinusoid, whose duration and amplitude can be modified to represent different compliances and heart rates. Thus, the ventricular pressure may be solved for, given that the flow rate at the root of the aorta is equal to the time derivative of ventricular volume.

Sinuses of Valsalva. As flow begins to reverse, the valve leaflets are swept backward and close without sustaining a significant pressure gradient. Filling of the sinuses continues until the valve leaflets are maximally distended, at which time the leaflets are able to sustain a pressure gradient. This may be modeled as an abrupt decrease in the aortic root compliance to a new value C_{sinus} as well as imposing a zero-flow boundary condition at the first node. This condition is held until the ventricular pressure again exceeds aortic pressure.

Terminal Branch Points. The numerical model described here uses linear segments to represent the larger vessels in the main arterial tree, but modeling the finer branching structure approaching the arterioles in this manner is impractical. Rather, the terminal vessels are modeled as a lumped parameter Windkessel.[9,8] The model allows the behavior of the small arterial vessel beds to be captured using only a few parameters and accurately mimics peripheral wave reflections.[18] The Windkessel consists of a resistance R_s in parallel with a compliance C_s, where the resistance represents the pressure drop associated with the terminal arterioles, and the compliance represents the total compliance of the small artery network. In series upstream from the Windkessel is an additional element Z_0, which represents the entrance impedance of the small arterial bed with an associated pressure drop of $P-P_c$, where P is the pressure at the last node in the terminating arterial segment, and P_c is the capillary bed pressure. This impedance is matched to that of the adjoining element to avoid the generation of reflections resulting from an impedance mismatch at this interface. Thus, Z_0 is approximated as $\rho c/A$ using the wave speed and area for the element node bordering the Windkessel. From the electrical analog, the following equations may be written as a function of the resistances and capacitances:

$$\frac{P_c - P_v}{R_s} + C_s\frac{dP_{\text{tm}}}{dt} = Q, \tag{16}$$

$$Q = \frac{1}{Z_0}(P - P_c), \tag{17}$$

where Q is flow entering the Windkessel, P_v is the venous pressure, and $P_{\text{tm}} = P_c - P_e$ is the transmural

pressure, where the external pressure P_e may be specified. The Windkessel is coupled numerically to its upstream element in this model using the method of characteristics.

Within the region of external compression the externally applied pressure is used as the reference pressure for the capacitor in the Windkessel model. Venous pressure is assumed constant for the purpose of these calculations. Consequently, the dynamics occurring on the venous side of the circulation, while potentially important, are not considered in the present calculations. The implications of this assumption are discussed later.

The model, as implemented for these simulations, is operated in "open mode" in that the venous and pulmonary circulations have been omitted. In so doing, the dynamics of the venous bed associated with EECP are essentially ignored on the assumption that the changes in mean venous pressure due to EECP will have minimal effect on the *pulsatile* flows and pressures on the arterial side. Variations of venous pressure in the region of compression may have a somewhat greater effect as discussed below.

Parameter Specification. Information on cardiovascular system parameters exists, but the data are highly variable and extremely dependent on the state (e.g., posture) of the individual or animal at the time when measurements are taken. Nonetheless, a standard case that produces a reasonable model output for a given set of parameters is required. Avolio[5] presents an extensive list of arterial lengths, diameters, wall thicknesses, and Young's moduli for most of the major human arteries (a sum total of 128). For the present model, 30 elements are used. This network is shown schematically in Fig. 1. The numbered elements correspond to major arteries whose properties are provided in Table 2.

Arterial elements were specified in the model by a proximal and distal internal radius, from which the cross-sectional areas were calculated. The area was assumed to be a linear function of length between bifurcations. All elements were discretized into nodes, separated by a spatial increment, nominally 0.01 m. The branching pattern of the arteries was also taken from the arterial tree layout given by Avolio.[5] In addition to geometrical measurements, the elasticity of each artery segment is specified in order to calculate the nominal reference wave speed c_0 for each element, using the Moens–Korteweg equation

$$c_0 = \sqrt{\frac{Eh}{2\rho R}}. \tag{18}$$

Here, c_0 depends locally upon Young's modulus E, inner radius R, fluid density ρ, and wall thickness h. Both R and h were assumed known with the internal static reference pressure P_0 equal to 100 mm Hg (13.3 kPa). Assuming a linear relationship between wall thickness and vessel radius, the model calculates c_0 at each node given dimensions and material properties. Values for Young's modulus (Table 2) were also obtained from Avolio's original data.

Local regulation of flow is extremely transient and dependent on a variety of factors, complicating the task

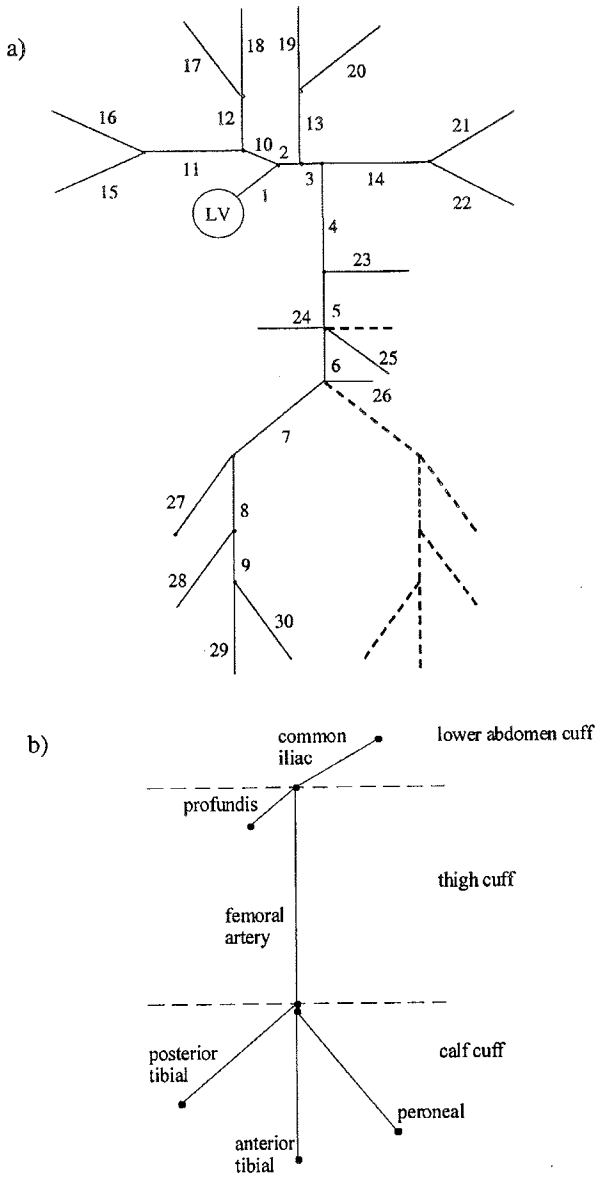

FIGURE 1. (a) The 30 element model of the arterial system. Dashed elements represent those that are reflected by symmetry and are not explicitly computed. (b) Division of lower arterial tree elements into three pressurization regions for EECP model. Figure is drawn to scale.

TABLE 2. Specifications for the 30 element model arterial properties. Proximal and distal cross-sectional areas are given, and it is assumed that area varies linearly with distance along the vessel. *E* is the Young's modulus of the vessel wall.

Element No.	Artery name	Length (m)	Proximal area ($\times 10^{-4}$ m^2)	Distal area ($\times 10^{-4}$ m^2)	$E \times 10^5$ (Pa)
1	ascending aorta	0.055	6.605	3.941	4.0
2	aortic arch	0.02	3.90	3.90	4.0
3	aortic arch	0.02	3.80	3.80	4.0
4	thoracic aorta	0.185	3.597	2.835	4.0
5	abdominal aorta	0.043	2.378	2.378	4.0
6	abdominal aorta	0.096	1.021	1.021	4.0
7	common iliac	0.192	0.849	0.229	4.0
8	femoral artery	0.432	0.181	0.126	8.0
9	anterior tibial artery	0.015	0.053	0.053	16.0
10	brachiocephalic	0.024	1.208	1.208	4.0
11	r brachial	0.410	0.503	0.181	4.0
12	r common carotid	0.168	0.503	0.503	4.0
13	l common carotid	0.110	0.503	0.503	4.0
14	l brachial	0.444	0.554	0.181	4.0
15	r radial	0.229	0.08	0.08	8.0
16	r ulnar	0.232	0.139	0.113	8.0
17	r external carotid	0.113	0.196	0.071	8.0
18	r internal carotid	0.172	0.283	0.053	8.0
19	l internal carotid	0.172	0.283	0.053	8.0
20	l external carotid	0.113	0.196	0.071	8.0
21	l radial	0.229	0.08	0.08	8.0
22	l ulnar	0.232	0.139	0.113	8.0
23	coeliac	0.010	0.478	0.478	4.0
24	renal	0.027	0.212	0.212	4.0
25	sup mesenteric	0.054	0.581	0.581	4.0
26	inf mesenteric	0.045	0.08	0.08	4.0
27	profundis	0.121	0.166	0.166	16.0
28	post tibial	0.306	0.102	0.102	16.0
29	ant tibial	0.295	0.031	0.031	16.0
30	peroneal	0.313	0.053	0.053	16.0

of defining a "standard" distribution of flow. An alternative approach used in this model is based on the observation that the caliber of a vessel is related to the flow rate it conveys. This was first proposed by Murray in 1926 and later shown to result from biological factors that tend to maintain a constant wall shear stress in all arteries.[13] Thus, assuming a blood viscosity of 4.0 $\times 10^{-5}$ kg m^{-1} s^{-1}, and a mean wall shear stress of 1.5 N m^{-2} at a mean arterial pressure of 13.3 kPa (100 mm Hg), the required flow can be calculated for each node within the network. The difference in flow between nodes is described by Eq. (4). From the calculated required flow at each distal boundary node, the appropriate value of the terminal Windkessel resistance R_s is determined for each terminal element. This method provides values of mean flow rate that are in reasonable agreement with known physiological values. Where the predicted values differ from literature values, adjustments have been made. Values of other hemodynamic parameters are shown in Table 3.

A base state was chosen, typical of conditions used clinically, from which the effects of various parameter variations could be studied. All data presented are taken from the tenth heart cycle of the model to ensure that the simulation has reached a steady state. A heart rate of 72 beats/min is used for all simulations. Values of the control parameters used for this base state are given in Table 3. Some judgement was exercised in parameter selection. A second set of parameter values, with peak ventricular contractility reduced from 6000 to 1000 dyn/cm^5, systemic vascular resistance increased from 1000 to 2666 dyn/cm^5, and end diastolic volume increased from 120 to 280 ml was used to simulate a patient with compromised ventricular function. Validation of the model with normal parameters included comparisons to measured wave forms at various locations in the arterial system and measured arterial input impedance. Comparisons were also made to pressure and velocity traces found in the literature, but since these vary considerably among individuals direct comparisons are of limited value. These can be found in Ozawa.[18]

TABLE 3. External pressurization input control parameters. All times referenced to the beginning of cardiac systole.

Parameter	Description	Baseline values
T_{infl}	Time from onset of cardiac cycle at which pressure starts to rise	0.20 s
T_{defl}	Time to begin deflation of cuffs from maximum external pressure	0.72 s
T_{card}	Period of cardiac cycle	0.86 s
P_{calf}	Maximum external pressure applied to calf vessels	200 mm Hg
P_{th}	Maximum external pressure applied to thigh vessels	150 mm Hg
P_{la}	Maximum external pressure applied to lower abdomen vessels	100 mm Hg
Δt_{seg}	Time interval between inflations of adjacent cuff regions with the distal region always pressurized first	0.03 s
t_{ramp}	Time it takes pressure to rise to and fall from its maximum value	0.03 s
ΔP_{seg}	Pressure difference between cuffs (pressure always increasing in the direction of the foot)	50 mm Hg
P_m	Average applied pressure in the three cuff regions	150 mm Hg

External Pressurization Scheme. A three-step *graded-sequential* compression procedure was employed in all the simulations presented here. In sequential compression, a wave of compression is applied to the vessels by inflating the three pressurization cuffs for the calves, thighs, and lower abdomen sequentially from ankle to groin. The pressure level applied by the cuffs decreases from calf to thigh, and from thigh to lower abdomen cuffs. In contrast to the emptying behavior characteristic of uniform compression, *sequential compression* produces a collapse in the vessels that proceeds from the foot toward the heart. Thus, the blood is effectively "milked" from the vessels in the lower extremities and does not pass through a constrictive throat as in uniform compression.[17] In *graded compression* the maximum level of pressure attained in each segment is greatest in the periphery and falls in the direction of the heart. The application of graded compression also helps to eliminate the occlusive throat and, in combination with sequential pressure application, produces rapid and complete emptying of the vessels.[17,30]

The cuffs used to provide pressurization of the lower extremities in EECP are modeled as external pressure sources on the lower abdomen, thigh, and calf arteries. To simulate graded-sequential compression in the model, the arterial tree elements for the lower body are divided into three regions, shown in Fig. 1, representing the areas covered by the three pressurization cuffs in EECP.

External Pressurization Control Parameters. Clinical and computational studies have shown the efficacy of EECP depends upon the mode of operation and parameter values used to control the device.[6] These parameters include the cuff inflation and deflation timings, the maximum pressure level applied externally to the vessels by each cuff, and the time delay of pressurization and depressurization between the calf, thigh, and lower abdomen cuffs for sequential compression. Table 3 shows a detailed description of the individual input control parameters governing external pressurization in the model.

In clinical practice, the application of external pressure during EECP is timed with the patient's electrocardiogram. In the EECP model, this process is accomplished by adjusting the timing of applied external pressure in each of the three compartments relative to left ventricular contraction, as characterized by $E(t)$. For graded-sequential compression, the pressure in each cuff rises linearly to its maximum value over a time t_{tramp}, is held constant until a time T_{defl}, and then falls linearly over a time t_{ramp} (see Fig. 2). The calf, thigh, and lower abdomen cuffs are inflated at times T_{infl}, $T_{infl}+\Delta t_{seg}$, and $T_{infl}+2\Delta t_{seg}$, respectively. The maximum applied pressure is decreased between the calf and thigh cuffs and the thigh and lower abdomen cuffs as specified by

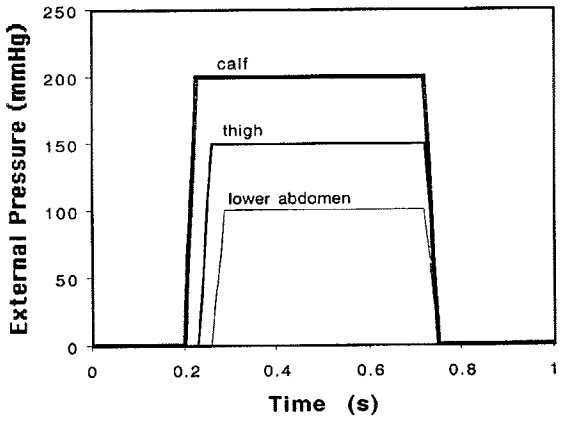

FIGURE 2. Application of external pressure with time during the heart cycle. Parameter values as given in Table 3.

P_{calf}, P_{th}, and P_{la}. The cuff deflation time, T_{defl}, is the same for all three cuffs to simplify the parameter study. The parameters used in the temporal application of external pressure during the heart cycle are given in Table 3. For all other parameter values, see Ozawa.[18]

Mean applied pressure was chosen at a level thought to produce minimum trauma to the patient while still providing a reasonable measure of benefit. The pressure increment between segments was viewed as sufficient to prevent proximal arterial collapse and a consequent impairment of vessel emptying while still providing ample pressure at the lower abdomen region to produce significant emptying. Consistent with the notion that arterial emptying should proceed at a speed comparable to the speed of the arterial pressure pulse (about 8 m/s in the peripheral arteries), the time delay between segment compressions was chosen to be approximately equal to the wave transit time through each of the pressurized compartments. Pressure rise time, as shown by Bai *et al.*, should be as short as possible.[7] Therefore, a value was chosen close to the practical lower limit.

External Pressurization Measures of Merit. The effectiveness of enhanced external counterpulsation is assessed in terms of the following measures of merit:

Mean Diastolic Pressure (MDP). The increase in diastolic pressure, or diastolic augmentation, is characterized by the mean diastolic pressure ratio

$$\mathrm{MDP}=\frac{\left[\frac{1}{T_D-T_S}\int_{T_S}^{T_D}P_{\mathrm{aortic}}dt\right]_{\mathrm{compr}}-\left[\frac{1}{T_D-T_S}\int_{T_S}^{T_D}P_{\mathrm{aortic}}dt\right]_0}{\left[\frac{1}{T_D-T_S}\int_{T_S}^{T_D}P_{\mathrm{aortic}}dt\right]_0}, \tag{19}$$

where P_{aortic} is pressure at the aortic root, T_D and T_S are the times at which diastole and systole, respectively, end, and the subscripts "compr" and "0" refer to cases with and without external compression, respectively. MDP is an indication of how diastolic pressure is increased with pressurization. All pressures are measured when the model has reached steady state after ten heart cycles.

Mean Systolic Pressure (MSP). The effect of EECP on systolic pressure is quantified using the mean systolic pressure ratio:

$$\mathrm{MSP}=\frac{\left[\frac{1}{T_S}\int_0^{T_S}P_{\mathrm{aortic}}dt\right]_0-\left[\frac{1}{T_S}\int_0^{T_S}P_{\mathrm{aortic}}dt\right]_{\mathrm{compr}}}{\left[\frac{1}{T_S}\int_0^{T_S}P_{\mathrm{aortic}}dt\right]_0}, \tag{20}$$

MSP is a measure of the extent of left ventricular afterload reduction with pressurization.

Emptying Effectiveness (EE). The blood volume emptied from the leg vessels enters the aorta, and hence determines the amount of diastolic augmentation achieved by EECP. It also provides a measure of the extent to which arterial diameter changes, and therefore relates to vessel wall strain. The emptying effectiveness parameter EE is used to measure the efficiency of the emptying process for the vessels receiving pressurization. EE is calculated for a single vessel using the equation

$$\mathrm{EE}=\frac{[\int A\cdot dx]_0-[\int A\cdot dx]_{\mathrm{compr}}}{[\int A\cdot dx]_0}, \tag{21}$$

where A is the cross-sectional area of the artery. The integrations are taken over the entire region of pressurization for the artery of interest. For the "compr" case, arterial area is measured at maximum pressurization in diastole just prior to cuff deflation. The arterial area for case "0" is measured at the time step just preceding pressurization. Thus, the emptying effectiveness of the artery represents the extent of arterial collapse under maximum pressurization with respect to the state of the artery just prior to pressurization. The state of the artery prior to pressurization is considered since the artery may be partially collapsed if there has not been sufficient time for it to completely refill.

Shear Stress Index. An approximate measure of shear stress is defined, which accounts for the changes in cross-sectional area and flow velocity that accompany EECP. In the case of steady, fully developed, laminar flow through a vessel of circular cross section, wall shear stress could be computed as follows:

$$\tau_w=\mu\frac{4\bar{V}}{\sqrt{A/\pi}}, \tag{22}$$

where $\bar{V}$ is the mean flow velocity. Recognizing that as an artery collapses, its cross section will likely deviate from circular, and that the flow is clearly not fully developed nor steady, we will still assume to a rough approximation that

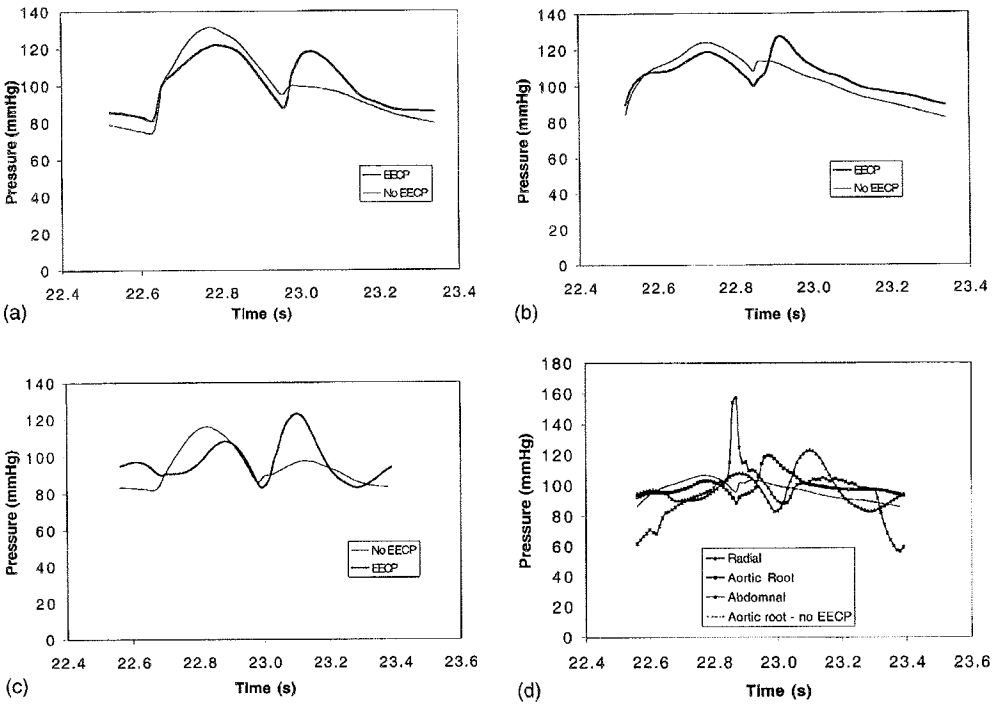

FIGURE 3. Pressure at several locations in the arterial tree with normal parameter values ("normal") and parameter values simulating compromised ventricular function ("diseased"). One complete cardiac cycle at steady state is shown, beginning with the onset of systole. Parameter values as given in Table 3. Greater augmentation, as evidenced by greater values of the effectiveness ratio, is seen in the simulated disease cases. (a) Radial artery, normal; (b) aortic root, normal; (c) radial artery, diseased; (d) radial, aortic root, and abdominal pressures, diseased.

$$\tau_w \propto \mu \frac{\bar{V}}{\sqrt{A}}. \tag{23}$$

Actual values of shear stress will be larger than this due to the change in vessel shape and unsteadiness. However, as these effects are difficult to estimate accurately without resorting to fully three-dimensional calculations, we have chosen instead to use Eq. (23) for the purpose of estimating the relative values of shear stress between simulations with and without EECP. Accordingly, a shear index S is defined as

$$S = \frac{\Sigma_{n=1}^{3} \bar{\tau}_{w,\text{compr}} - \Sigma_{n=1}^{3} \bar{\tau}_{w,0}}{\Sigma_{n=1}^{3} \bar{\tau}_{w,0}}, \tag{24}$$

where $\bar{\tau}_{w,\text{compr}}$ is the time integral of the wall shear stress for one cycle evaluated at the midpoint of the compression zone and $\bar{\tau}_{w,0}$ is the same value with no external pressurization. The summation sign indicates that the values of $\bar{\tau}_{w,\text{compr}}$ and $\bar{\tau}_{w,0}$ are summed over the three compression zones.

RESULTS

Pressure pulses at the radial artery and aortic root computed by the model (Fig. 3) with and without graded-sequential external compression from the lower abdomen to the foot clearly illustrate the hemodynamic effects of EECP. Compression of a "normal" subject [Fig. 3(a)] is contrasted to EECP in a patient with reduced ventricular function [Fig. 3(b)]. In both cases, pressure is applied by a three-compartment cuff with maximum pressures of 200, 150, and 100 mm Hg along the lower leg, upper leg, and lower abdomen, respectively. Note that in this instance of arterial counterpulsation (pressure application during cardiac diastole and release of pressure during systole) systolic pressure is reduced while diastolic pressure is augmented, leading to the combined effects of reduced ventricular afterload and enhanced coronary blood flow.

The effectiveness of EECP can be viewed in terms of the measures of merit defined previously. These results, computed for the "normal" subject, are shown in Table 4. Numbers shown in the table correspond to the fractional change in each measure from the case without

TABLE 4. Values for each of the measures of merit for the baseline conditions given in Table 3.

	Values under baseline conditions
MDP	0.0782
MSP	0.0238
EE	0.373
S	3.22

compression and are defined so that they range in value from zero (no effect) to order one.

For this same condition of external compression, the time-varying arterial cross-sectional area and a measure proportional to the time-varying shear stress [see Eq. (23)] are plotted for three locations (lower abdomen, thigh, and calf) in Figs. 4 and 5. During pressure application, the arteries collapse with sufficient speed to cause a flow reversal throughout much of the arterial network and a significant increase in vascular shear stress in the arteries of the lower extremity. The arteries in the lower abdomen and thigh [Figs. 4(a) and 4(b), respectively] refill rapidly upon pressure release, even rising to slightly above normal levels due to the strong compression wave generated and its reflection from the peripheral vascular bed. During refilling, shear stress attains levels roughly three- to four-fold higher than under normal conditions at all three locations (Fig. 5). Features of particular interest in the context of endothelial function are the high shear stresses of reversing sign, and the significant arterial wall strain due to arterial collapse.

One way to elucidate the relative effects of the various compression parameters is by the sensitivity matrix of Table 5. Considering that each measure of merit (MM) (e.g., MDP) is a function of each of the adjustable parameters (Y) (e.g., mean applied pressure), then an entry in the table (X) represents the change in the measure of merit [Δ(MM)] divided by the fractional change in the parameter value

$$X = \frac{[\Delta(\mathrm{MM})/\mathrm{MM}_{\mathrm{mean}}]}{[\Delta Y/Y_{\mathrm{mean}}]}. \tag{25}$$

Large values indicate strong correlations between the MM and the particular parameter. For example, a 10% increase in mean applied pressure P_m will produce an increase of 0.0078 (=0.1 1.01 0.0782) in MDP. This table is useful for identifying the parameters that, when varied, will have the greatest influence on the measure of interest.

While the dependencies are generally quite symmetric about the baseline case, suggesting a nearly linear dependence, there is one notable exception. The time to initiate cuff inflation T_{infl} selected for the baseline case was near the optimum in terms of reducing mean systolic pressure. Thus, although T_{infl} has a strong influence on most of the MM, increasing or decreasing it by small amounts from the baseline case does not appear to have much effect on MSP. Changes of larger magnitude, however, will have significant deliterious effects; e.g., if cuff inflation occurs earlier, before the end of systole, systolic unloading will be severely affected.

Mean applied pressure clearly has the greatest potential to enhance diastolic pressure and increase levels of shear stress, although increasing mean pressure probably has the largest *negative* impact on patient tolerance. Altering cuff inflation time also exerts an important influence, although some of its effects are counterproductive (e.g., when S and EE increase, MDP falls). Reducing pressure rise time (t_{ramp}) is also beneficial, although this may be difficult to accomplish in practice.

DISCUSSION

The simulations of EECP presented here, provide insight into the dynamic processes that accompany EECP. Beginning near the end of systole, compression produces arterial collapse, sending a wave of retrograde flow up into the aorta, increasing pressure up as far as the aortic root and, presumably, augmenting coronary blood flow. When compression is released near the end of diastole, the arteries begin to refill, initiating a rarefaction wave that propagates toward the heart, reaching it at a time that produces systolic unloading. The extent of emptying of the leg arteries decreases toward the periphery, but corresponds to approximately half their normal arterial volume within the range of pressures tested here. Refilling to normal volumes is achieved in the most proximal arteries, but even at the levels of pressure used in these simulations, is incomplete in the lower leg. Increasing pressure applied to the calf up to 300 mm Hg (results not shown) compromises refilling even further. The results in Table 3 demonstrate the potential for controlling mechanical events related to cardiac assist or vascular cell stimulation, and perhaps more importantly, show that optimization of the measures relating to cardiac function is not always consistent with optimization of the vascular stimulus.

In previous models of EECP, the arteries were represented as a collection of lumped elements and were therefore not capable of accurately capturing many of the phenomena associated with wave propagation through the arterial network and arterial collapse.[6,7] The present model, although still discretized, solves the distributed differential equations and also incorporates the nonlinearities associated with arterial collapse and convective acceleration which are critical under conditions of EECP. Consequently, the model captures the influence of for-

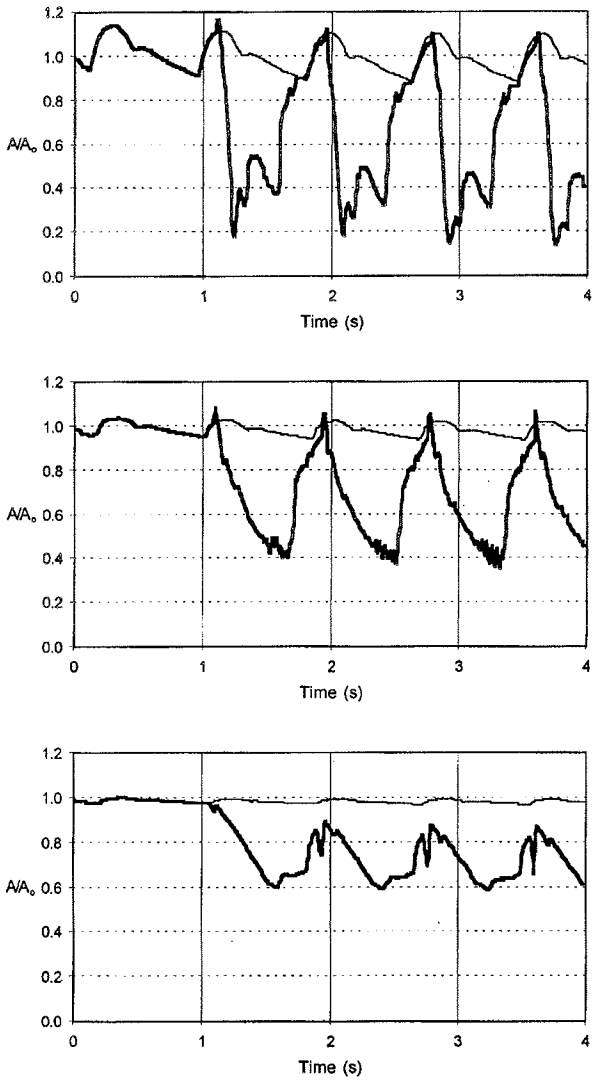

FIGURE 4. Cross-sectional area plotted vs time for several cardiac cycles following the onset of EECP at the midpoint of the: (a) lower abdomen, (b) thigh, and (c) calf compression zones, respectively, normalized with respect to the cross-sectional area without external compression at 100 mm Hg (A_0): (light lines) no external compression, (dark lines) with external compression.

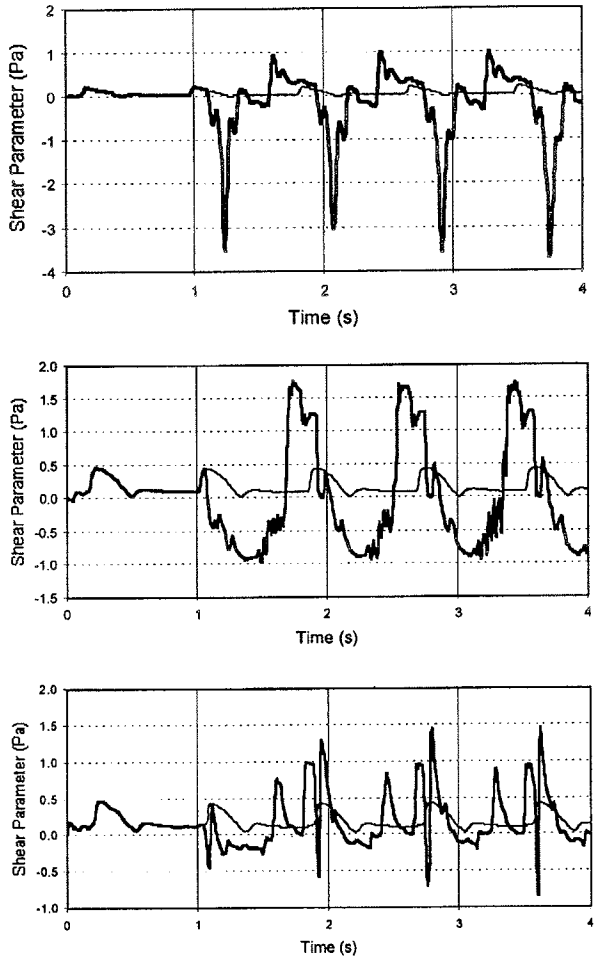

FIGURE 5. A measure of arterial wall shear stress [Eq. (23)] plotted vs time for several cardiac cycles following the onset of EECP at the midpoint of the: (a) lower abdomen, (b) thigh, and (c) calf compression zones, respectively. Magnitude is increased by more than three-fold (much more in the lower abdomen) and flow reversal is evident: (light lines) no external compression; (dark lines) with external compression. Note that mean shear stress in the normal arterial circulation is generally in the range of 1.5 Pa.

ward and backward propagating waves, can reproduce the complex impedance of real arterial networks,[18] and thereby provides a means to examine the detailed flow dynamics associated with EECP. As seen in Fig. 4, the onset of compression at the lower leg sends a surge of blood toward the heart, producing the rapid rise in cross-sectional area in the thigh [see e.g., $t=3.60$ s in Fig. 4(b)] and the lower abdomen [$t=3.64$ s in Fig. 4(a)] just prior to compression of these regions. The abrupt fall in cross-sectional area in the calf [beginning at $t=3.56$ s, Fig. 4(c)] is followed by an equally abrupt rise in area,

TABLE 5. Sensitivity matrix. Each numerical value represents the fractional change in the particular measure of merit [Δ(MM)/MM$_{mean}$] divided by the fractional change in the parameter [$\Delta Y/Y_{mean}$] as defined in Eq. (25). Note that a positive value indicates an increase in magnitude of the measure of merit for a positive change in the parameter.

$Y=$	P_M	ΔP_{seg}	t_{ramp}	Δt_{seg}	T_{infl}
MDP	1.01	−0.140	−0.107	−0.086	−0.887
MSP	1.26	−0.512	−0.147	0.067	−0.059
EE	−0.614	0.236	−0.075	−0.029	0.702
S	2.82	−0.193	−0.028	0.107	0.616

before the area decreases more consistently as pressure is maintained. The low frequency oscillation occurring in the iliac artery [$t=2.9-3.2$ s, Fig. 4(a)] is evidence of wave reflection from the proximal end of the aorta, causing some refilling while pressure is still maintained. These waves are highly damped, however, and are not seen in the thigh or calf regions.

These results, in terms of the magnitude of the effect observed in arterial blood flow and pressure, can to some extent be compared with previous observations. In the multicenter study, the hemodynamic effects of EECP were monitored by determining an "effectiveness ratio" defined as peak diastolic pressure minus end-diastolic pressure divided by peak systolic pressure minus end-diastolic pressure.[4] Using the aortic blood pressure trace, this ratio is 0.90 for our standard case [Fig. 3(b)] and 1.60 for the case with a compromised ventricle ("diseased") simulation [Fig. 3(d)] compared to an average of 1.41 ± 0.51 in the multicenter trial. Note that the patient values: (1) were based on measurements with a finger plethysmograph and therefore are not directly comparable to our predictions and (2) were obtained using maximum pressures up to 300 mm Hg. In a separate study, most effects (e.g., change in cardiac output, ratio of retrograde to antegrade aortic flow) had nearly reached their maximal effect when the diastolic-to-systolic pressure ratio attained values in the range of 1–2.[27]

We chose to study a range of pressures below those currently used clinically in recognition of the relatively high number of adverse experiences reported by patients receiving EECP. In the multicenter study,[4] 54.9% of patients experienced adverse effects, with the majority of these being device related. The number of device-related adverse effects was reduced nearly fourfold (from 37 to 10) in a separate group of patients in whom applied pressures were decreased from 300 to 75 mm Hg. Our results indicate that significant hemodynamic effects, especially in terms of enhancing arterial shear stress and arterial wall strain, can be achieved with the use of considerably lower pressures, with mean values in the range of 150 mm Hg.

Our assumption of constant venous pressure has several potential implications. Consider first the effect of compression on the veins of the lower extremity. The magnitude and frequency of compression will almost certainly cause these veins to be in a state of collapse throughout the cycle since venous valves prevent rapid refilling as occurs on the arterial side. Thus, during compression, venous pressure will be at or slightly elevated above central venous pressure, but during the relaxation phase it will be strongly negative. We anticipate that this would lead to an increase in mean limb flow but of unknown magnitude. A second effect of compression, secondary to the collapse of the veins of the lower extremities, would be a slight elevation of central venous pressure leading to enhanced venous return and activation of the atrial baroreceptors. The effects of these changes are difficult to predict with the present model, and deserve further attention. For the purpose of predicting the pulsatile changes in flow and cross-sectional area in the leg arteries, however, these changes on the venous side should have relatively little impact. Several additional simulations (results not shown) were conducted with end diastolic volume increased by 20 ml, and with venous pressure increased 5 mm Hg. The latter produced results indistinguishable from those presented here. The increase in end diastolic volume led to an overall increase in arterial pressure by about 10 mm Hg, but the pressure profile with EECP changed very little. The net effect would be a reduction in systolic unloading and an increase in diastolic augmentation.

Another potential source of uncertainty relates to the values for elastic modulus used for the arterial tree. Although we used the only data we were aware of in the literature,[5] these are only estimates and are therefore subject to error. Since the stiffness of the arteries under collapse is based on these estimates, it is possible that the pressures required to produce a certain degree of arterial emptying may also be uncertain. Add to this the subject-to-subject variability likely to be present, and it is apparent that these results should be used only as a rough guide to estimating the parameter values for any particular subject, and that some amount of empirical testing is essential in practice.

It is interesting to note that recent clinical results show benefits in cardiac function from as little as 1 h of treatment per day. Under this protocol, Lawson *et al.* found that 17 out of 18 patients receiving EECP for as little as 36 1 h treatments reported improvement in anginal symptoms, despite prior medical and surgical therapy.[15] The results of the recent multicenter study involving 139 patients confirmed these findings and showed that EECP reduces exercise-induced ischemia and angina.[4] A 1996 study by Lawson *et al.* also showed improved exercise tolerance in 22 out of 27 patients with chronic stable angina.[16]

While the mechanism by which patients accrue benefit from EECP treatments remains unclear, evidence points to the importance of factors other than the obvious mechanical ones that prompted early studies of EECP as an external cardiac assist method. It is now thought that the benefits of EECP may be related to the recruitment of collateral vessels in the coronary circulation, perhaps due to an increase in the synthesis and release of vascular growth factors.[21]

Recently, Soran *et al.* have proposed that EECP may act by altering endothelial function due to changes in the level of shear stress in the arteries.[21] Although EECP has been shown to increase the perfusion through the carotid

and renal arteries by approximately 20% in one study,[3] the effects of elevated shear on the synthesis and release of various cytokines and growth factors are clearly not restricted to the coronary vascular bed. Shear stress is elevated throughout much of the arterial system, especially in the arteries of the lower extremities by a combination of flow augmentation and reduced arterial cross-sectional areas, producing levels of shear stress up to more than four times normal values. These high levels of shear occur during both antegrade and retrograde flow (Fig. 5). While potentially damaging to the endothelium, these high shear stresses might also provide benefit by stimulating the release of shear-induced angiogenic factors from the arterial endothelium of the lower extremities.[12,26] This has not previously been considered and clearly deserves further study.

In terms of designing optimal protocols for EECP, it is critically important to understand the mechanism by which myocardial function is improved. In particular, parameter variations that optimize the traditional measures of merit (reduction in systolic pressure and increase in diastolic pressure) are not always consonant with the desire to maximize the magnitude and spatial extent of changes in arterial shear stress in the lower extremity. These issues will need to be better understood before a rationale design of the EECP protocol is possible.

ACKNOWLEDGMENTS

The authors would like to thank Aircast, Inc. for their financial and technical support in this research and acknowledge fellowship support received by Edwin T. Ozawa and Karen E. Bottom from the National Science Foundation and by Edwin T. Ozawa from the Harvard/MIT Division of Health Sciences.

REFERENCES

[1] Amsterdam, E. A. *et al.*, Clinical assessment of external pressure circulatory assistance in acute myocardial infarction. *Am. J. Cardiol.* 45:349–356, 1980.

[2] Anderson, D. A., J. C. Tannenhill, and R. H. Pletcher, Computational Fluid Mechanics and Heat Transfer. New York: McGraw Hill, 1984.

[3] Applebaum, R. M., R. Kasliwal, P. A. Tunick, N. Konecky, E. Katz, N. Trehan, and I. Kronzon. Sequential external counterpulsation increases cerebral and renal blood flow. *Am. Heart J.* 133:611–615, 1997.

[4] Arora, R. R., T. M. Chou, D. Jain, B. Fleishman, L. Crawford, T. McKiernan, and R. W. Nesto. The multicenter study of enhanced external counterpulsation (MUST-EECP): Effect of EECP on exercise-induced myocardial ischemia and anginal episodes. *J. Am. Coll. Cardiol.* 33:1833–1840, 1999.

[5] Avolio, A. P.. Multi-branched model of the human arterial system. *Med. Biol. Eng. Comput.* 18:709–718, 1980.

[6] Bai, J., D. Wu, and J. Zhang. A simulation study of external counterpulsation. *Comput. Biol. Med.* 24:145–156, 1994.

[7] Bai, J., K. Ying, and D. Jaron. Cardiovascular responses to external counterpulsation: A computer simulation. *Med. Biol. Eng. Comput.* 30:317–323, 1992.

[8] Berger, D. S., J. K.-J. Li, and A. Noordergraf. Differential effects of wave reflections and peripheral resistance on aortic blood pressure: A model-based study. *Am. J. Physiol.* 266:35:H1626–H1642, 1994.

[9] Berger, D. S., J. K.-J. Li, and A. Noordergraf. Arterial wave propagation phenomena, ventricular work, and power dissipation. *Ann. Biomed. Eng.* 23:804–811, 1995.

[10] Bottom, K. E. A numerical model of cardiovascular fluid mechanics during exernal cardiac assist. S.M. thesis. Massachusetts Institute of Technology, May 1999.

[11] Holenstein, R., P. Niederer, and M. Anliker. A viscoelastic model for use in predicting arterial pulse waves. *J. Biomech. Eng.* 102:318–324, 1980.

[12] Hseih, H. J., N. Q. Li, and J. A. Frangos. Shear stress increases endothelial platelet-derived growth factor mRNA levels. *Am. J. Physiol.* 260:H642–H646, 1991.

[13] Kamiya, A., R. Bukhari, and T. Togawa. Adaptive regulation of wall shear stress optimizing vascular tree function. *Bull. Math. Biol.* 46:127–137, 1984.

[14] Kamm, R. D., and A. H. Shapiro. Unsteady flow in a collapsible tube subjected to external pressure or body forces. *J. Fluid Mech.* 95:1–78, 1979.

[15] Lawson, W. E. *et al.*, Efficacy of enhanced external counterpulsation in the treatment of angina pectoris. *Am. J. Cardiol.* 70:859–862, 1992.

[16] Lawson, W. E., J. C. Hui, Z. S. Zheng, L. Burgen, L. Jiang, O. Lillis, Z. Oster, H. Soroff, and P. Cohn. Improved exercise tolerance following enhanced external counterpulsation: Cardiac or peripheral effect? *Cardiology* 87:271–275, 1996.

[17] Lueptow, R. M., J. M. Karlen, R. D. Kamm, and A. H. Shapiro. Circulatory model studies of external cardiac assist by counterpulsation. *Cardiovasc. Res.* 15:443–455, 1981.

[18] Ozawa, E. T. A numerical model of the cardiovascular system for clinical assessment of the hemodynamic state. PhD thesis. Massachusetts Institute of Technology, September 1996.

[19] Parmley, W. W., K. Chatterjee, Y. Charuzi, and H. U. Swan. Hemodynamic effects of noninvasive systolic unloading (nitroprusside) and diastolic augmentation (external counterpulsation) in patients with acute myocardial infarction. *Am. J. Cardiol.* 33:819–825, 1974.

[20] Pedley, T. J., R. C. Schroter, and M. F. Sudlow. Energy losses and pressure drop in models of human airways. *Respir. Physiol.* 9:371–386, 1970.

[21] Soran, A. U., L. E. Crawford, V. M. Schneider, and A. M. Feldman. Enhanced external counterpulsation in the management of patients with cardiovascular disease. *Clin. Cardiol.* 22:173–178, 1999.

[22] Sorroff, H. S., C. T. Cloutier, W. C. Birtwell, L. A. Begley, and J. V. Messer. External counterpulsation, management of cardiogenic shock after myocardial infarction. *J. Am. Med. Assoc.* 229:1441–1450, 1974.

[23] Stettler, J. C., P. Niederer, and M. Anliker. Theoretical analysis of arterial hemodynamics including the influence of bifurcations. Part I: Mathematical model and prediction of normal pulse patterns. *Ann. Biomed. Eng.* 9:145–164, 1981.

[24] Suga, H., and K. Sagawa. Instantaneous pressure-volume relationships and their ratio in the excised, supported canine left ventricle. *Circ. Res.* 35:117–126, 1974.

[25] Suga, H., K. Sagawa, and L. Demer. Determinants of instantaneous pressure in canine left ventricle: Time and volume specification. *Circ. Res.* 46:256–263, 1980.

[26] Sumpio, B. E.. Hemodynamic forces and the biology of the endothelium: signal transduction pathways in endothelial cells subjected to physical forces *in vitro*. *J. Vas. Surg.* 13:744–746, 1991.

[27] Suresh, K., S. Simandl, W. E. Lawson, J. C. Hui, O. Lillis, L. Burger, T. Guo, and P. F. Cohn. Maximizing the hemodynamic benefit of enhanced external counterpulsation. *Clin. Cardiol.* 21:649–653, 1998.

[28] Wolf, T. An experimental/theoretical investigation of parallel inhomogeneities in respiratory flows. PhD thesis. Massachusetts Institute of Technology, June 1990.

[29] Young, D. F., and F. Y. Tsai. Flow characteristics in models of arterial stenoses-II. Unsteady flow. *J. Biomech.* 6:547–559, 1973.

[30] Zheng, Z. S. *et al.*, Sequential external counterpulsation (SECP) in China. *Trans. Am. Soc. Artif. Intern. Organs* 29:599–603, 1983.